J. Fluid Mech. (2003), *vol.* 483, *pp.* 287–314. © 2003 Cambridge University Press
DOI: 10.1017/S0022112003004166 Printed in the United Kingdom

Double-diffusive transport in laboratory thermohaline staircases

By R. KRISHNAMURTI

Department of Oceanography and Geophysical Fluid Dynamics Institute, Florida State University, Tallahassee, FL 32306, USA

(Received 30 May 2002 and in revised form 31 December 2002)

Laboratory experiments were conducted on a double-diffusing fluid stabilized by the faster diffuser (T) and destabilized by the slower diffuser (S), the arrangement that leads to salt fingering. The experiments were conducted in three tanks of depths 2 m, 1 m or 0.3 m, with initial linear profiles of S and T between two reservoirs at fixed or known values, $S_0 + \Delta S$, $T_0 + \Delta T$ in the top reservoir, S_0, T_0 in the bottom reservoir.

In the thermohaline staircase regime consisting of an alternating stack of convecting layers and finger layers, the overall fluxes F_S and F_T are clearly not depth independent. The overall Nusselt number, N_S varies inversely with the number n of finger layers plus convecting layers occurring in the experimental fluid. The largest Nusselt number occurs for $n = 1$. The number n increases with increasing mean vertical gradient, up to a point. If the vertical gradients are large, n is always equal to 1.

Internal measurements show that in the Rayleigh number range $|R_S| \sim 10^{15}$ and density ratio range $R_\rho \sim 1.1$ to 1.2, the finger flux $F_S^f \sim (\delta S/h) R_S^a R_\rho^b$ with $a = 0.18$ to 0.19 and $b = 1.8$ to 2.1. The data show dependence of F_S^f on finger layer thickness h. In the convecting layers, $N_S^c \propto R^{0.21}$ for large enough aspect ratio.

1. Introduction

When the density, ρ, of a fluid is determined by two components such as temperature T and salinity S, which diffuse at different rates, flows can occur even when the fluid is statically stably stratified. This is a report on laboratory experiments on such a fluid, with the faster diffuser (T) stabilizing and the slower diffuser (S) destabilizing, with the density of the fluid increasing downwards. This is the arrangement in subtropical oceans (hot salty above, cold fresh below), which can result in salt-fingering instabilities. In laboratory experiments, however, sugar (the slower diffuser) is often used as a proxy for salt, and salt (the faster diffuser compared to sugar) is used as a proxy for cold. This avoids the usually uncontrolled heat exchange with the environment of the experiment. However, the faster diffuser is still labelled T, the slower diffuser labelled S.

The purpose of the experiments reported here was to determine a flux law that would express the vertical fluxes of salt and of heat in terms of external control parameters such as ΔS, the salinity difference and ΔT, the temperature difference between top and bottom of the fluid layer. Flux laws have long been known for a single salt-fingering layer or 'salt-finger interface,' that forms between an upper 'reservoir' which is hot and salty, and a lower 'reservoir' which is cold and fresh. Here ΔS and ΔT are prescribed or known from direct measurement. However, for a thermohaline staircase, consisting of many finger interfaces between convecting

layers, each finger layer has its own ΔS, ΔT, and layer thickness. These are usually not identical for each layer, are not prescribed, and are not known *a priori*. For such a system the single-interface flux laws will prove to be insufficient.

The clearest and most persistent result of past laboratory measurements of fluxes through a single finger interface is that the salt flux F_S is proportional to $(\Delta S)^{4/3}$ and that it is independent of any vertical length scale (Turner 1967; Linden 1973; Schmitt 1979; McDougall & Taylor 1984). This would imply that the salt Nusselt number N_S, defined as the ratio of F_S to the diffusive flux, must be proportional to the salt Rayleigh number R_S to the 1/3 power, where

$$N_S = F_S/\kappa_S(\Delta S/d),$$
$$R_S = g\beta\Delta S d^3/\kappa_T\nu,$$

and where κ_S is the salt diffusivity in water, κ_T the heat diffusivity in water, ν the kinematic viscosity of water, and $\beta = (\partial\rho/\partial S)/\rho_0$, the fractional change in density with a change in salinity S; ρ_0 is the reference density, g is the acceleration due to gravity, and d is the layer depth.

In Rayleigh–Bénard convection it appeared that the thermal Nusselt number N_T was proportional to the thermal Rayleigh number to the 1/3 power, at least in a range of R_T up to order 10^6 (Goldstein, Chaing & See 1990), where

$$R_T = g\alpha\Delta T d^3/\kappa_T\nu,$$
$$N_T = F_T/\kappa_T(\Delta T/d),$$

and where α is the thermal expansion coefficient, $\alpha = -(\partial\rho/\partial T)/\rho_0$ and F_T is the heat flux. There was considerable scatter in the data used to determine this power, part of the scatter being due to the differing aspect ratios of the different apparatus involved. The argument for the 1/3 power was that at large R_T, which would most likely mean large d, the fluid near the heated bottom boundary would not be responding to conditions far above it, but would transport heat in response only to conditions near the bottom boundary. Hence the heat flux F_T should be independent of d. Then it would follow that $N_T \sim R_T^{1/3}$. In counter-argument, it would seem that this might be true in an initial transient response, but ultimately if a steady state were achieved, then conditions from large d would surely affect the fluid near the bottom boundary.

More recent experiments have definitely shown that beyond $R_T \sim 10^6$ the exponent is not 1/3. An exponent of 0.28 is observed (Castaing *et al.* 1989) in a range of Rayleigh numbers of order 10^6 to 10^{12}, in tanks of aspect ratio A of order 1, where A is the ratio of width to depth of the tank, while an exponent of 0.25 or 0.20 is observed for A of order 10 or more (Krishnamurti 1995); the latter observations were limited to the Rayleigh number range 10^6 to 10^8. The exponent 0.25 was observed for Rayleigh numbers decreased from 10^8 (ramped down in small steps, between external steady states), while the exponent 0.20 was observed for Rayleigh numbers increased from 10^6. The hysteresis was related to the nature of the large-scale shearing flow that tends to persist through small changes in R_T. When the large-A tank was partitioned with rigid and insulating walls into multiple (specifically 144) domains each with $A = 1$, the exponent of 0.28 was recovered.

In the case of salt fingers, the flux might be independent of finger length if these fingers were acting like conduits or pipes, carrying salty (ΔS) fluid in the down-pipes, fresh ($S = 0$) fluid in the up-pipes, with negligible lateral salt diffusion. Increased finger length would not lead to a change in vertical velocity w if w were locally determined

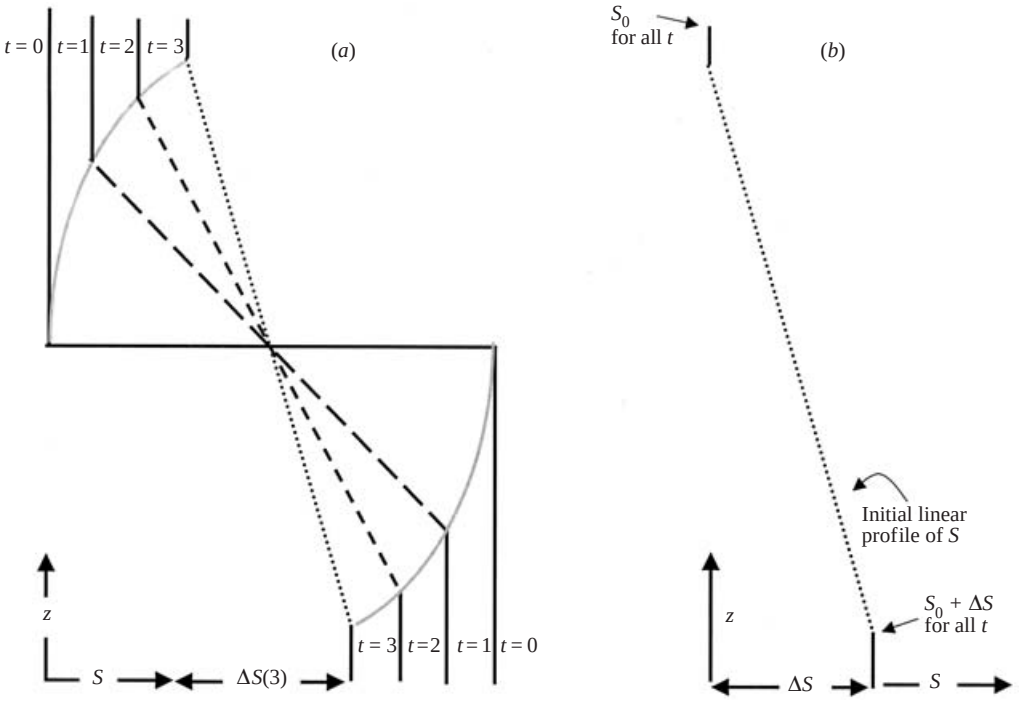

FIGURE 1. The relationship of the classical 'run-down' experiment to the 'initial linear profile between fixed reservoirs' experiment: (*a*) salinity profiles in the sugar–salt finger interface of a classical run-down experiment; (*b*) the salinity profile in a sugar–salt finger experiment with initial linear profile between fixed boundary values of S, provided a staircase does not form.

at each z by the buoyancy attained from lateral heat exchange. Then the salt flux $w\Delta S$ would be independent of depth.

If F_S were proportional to $(\Delta S)^{4/3}$ independent of depth d, then the same ΔS, ΔT imposed across our three tanks of depths 2 m, 1 m, 0.3 m should all have the same salt flux, and the Nusselt numbers should be in the ratio 2:1:0.3. We show below that this is far from the observed result. The fluxes were different for the three depths, for the same ΔS, ΔT imposed. Furthermore, it was the 0.3 m tank that had the greatest Nusselt number, even though it had the smallest Rayleigh number. This observation and explanation are elaborated below in terms of the number of salt-finger interfaces and convection layers that were found in the three tanks.

It should be mentioned that our experiments were not prepared as in most previous studies for the single finger interface, where the fingers grew on the interface between two water masses (or 'reservoirs'), eventually growing into and occupying more and more of the initial volume of these reservoirs. This is indicated schematically in figure 1(*a*). Instead, we start with a profile such as shown in figure 1(*b*). We have two fixed reservoirs of known salinity and temperature ($S_0 + \Delta S$, $T_0 + \Delta T$ in the top reservoir, S_0, T_0 in the bottom reservoir). The working fluid in the test section, which was prepared initially with linear gradients of T and S, lies between these reservoirs, with rigid porous membranes separating the test section from the reservoirs (see figure 2 below). Apart from these membranes, the arrangement resembles Linden's experiments (Linden 1978). Our test section has fixed height of 2 m or 1 m or 0.3 m. Linden's linear gradient region was 12 cm in height. When fingers filled the entire

depth of our test section, as they do in a certain parameter range, then there is a general geometrical similarity to the classical single-interface experiment. Thus, the profile in figure 1(*b*) was prepared to resemble that in figure 1(*a*) at time $t = 3$. In view of Turner's ingenious method of running through parameter space with the passage of time in his classical run-down experiments it would seem unwarranted to repeat these step by step, each with fixed boundary values, and this was not our aim. Rather, we used the initial linear profile method to make thermohaline staircases. The values of T, S in the reservoirs could be held fixed or allowed to decrease with time. It was found that in certain other parameter ranges, fingers do not fill the entire depth of the initial linear profile, but instead an alternating stack of finger layers and convection layers formed, as Linden (1978) had found. The flow in our test section could consist of 10 finger interfaces alternating in the vertical with 9 convecting layers in a depth of 2 m. It is the flux measurements in this regime that are reported in this paper.

Stern & Turner (1969) state that the flux law across one of these finger interfaces is of the same form as for the single interface; however, the magnitude of the drop ΔS_i, ΔT_i across the ith interface in general is not known since neither the number of interfaces nor their thicknesses are known *a priori*. In this paper we show the relationship between the overall Nusselt number and the number of finger interfaces.

It is tempting to think of these stacks of alternating finger layers and convecting layers as the laboratory analogue of the thermohaline staircase observed in subtropical oceans and especially pronounced in the Tyrrhenian Sea, where layers homogenous in T and S alternate with layers with steep gradients of T and S (Molcard & Williams 1975). Here, homogenous (convecting) layers typically tens to hundreds of metres deep separate the steep gradient (fingering) layers which are a few metres deep. However, within this steep gradient layer there may be sub-layers of fingers and convection, and it could be these that are being modelled in the laboratory.

It is strikingly clear in the oceanographic literature (see Kunze 1987 for discussion and references) that the laboratory 4/3 power flux law is inappropriate when applied to 2 m thick finger interfaces observed in the thermohaline staircase in the subtropical North Atlantic Ocean, east of Barbados. The 4/3 power law gives buoyancy fluxes $1\frac{1}{2}$ orders of magnitude larger than could be balanced by the measured dissipation rates. Theoretical models such as the Richardson number constraint of Kunze (1987), or the collective instability criterion of Stern (1969), limit the length that fingers may attain before becoming unstable. The resulting loss of vertical coherence in the disrupted fingers leads to lowered fluxes. However, from an instability theory of fingers one cannot easily guess if the resulting state is a staircase of alternating convection/finger layers, or a statistical ensemble of short, growing fingers.

The experiments described in this paper have not been designed to test theories, but rather simply to obtain flux laws in laboratory staircases. There appeared to be two clear avenues to explore. First, in the power law $N_S \sim |R_S|^a$, the exponent a might be different from 1/3 in previously unexplored ranges of R_S. Rayleigh numbers encountered in the sub-tropical oceans are negative and frequently of order $|R_S| \sim 10^{15}$ (using $|g(\Delta\rho/\rho)| \simeq 1 - 10$ cm s^{-2}; $\kappa_T \simeq 10^{-3}$ cm^2 s^{-1}, $d \simeq 10 - 100$ m.) At these Rayleigh numbers, a flux given by $N_S \simeq |R_S|^{1/3}$ differs by a factor of 100 from a flux given by $N_S \simeq |R_S|^{0.20}$. In this paper we determine values of a for each interface, but a sensible law could not be found in terms of the overall R_S, which was of order 10^{11} to 10^{15} in our experiments. This may be related to the fact that the Rayleigh numbers have internal reversals of sign, being negative across each finger layer and positive across each convecting layer.

The second avenue to explore was the loss of vertical coherence in fingers when they are stirred by convection layers. Pursuing this approach, we find a smaller F_S and N_S with larger n, where n is the number of finger interfaces across the fluid.

Our hope was that laboratory-determined flux laws might be useful in determining the double-diffusive modification of the temperature and salinity of seawater at depth, under the influence of surface heating and evaporation. It is this modified seawater that participates in the global thermohaline circulation; in the North Atlantic Ocean, upper-layer subtropical waters flow slowly northward to replace the coldest polar waters that sink, forming the southwards flowing North Atlantic Deep Water. The flux law for the vertical exchange of temperature and salinity between these opposing currents will ultimately be needed to compute the poleward fluxes of heat and salt.

2. Apparatus

A schematic diagram of the apparatus is shown in figure 2. Three such tanks were used, all constructed alike out of Plexiglas, except that the three had different test section heights of 183 cm, 91 cm, and 30 cm. These will be called, for convenience, the 2 m, the 1 m, and the 0.3 m tanks respectively. Each tank consists of three segments: the bottom reservoir, the test section, and the top reservoir. Porous membranes separate the three segments. In all three tanks both top and bottom reservoirs were 30 cm deep. The inside dimensions in horizontal cross-section were 30 cm by 10 cm, for reservoirs and test-sections alike. The Plexiglas walls were 1.9 cm thick.

Each reservoir had a Teflon-coated magnetic stirring bar, mounted on an acrylic cradle attached to a shaft that was free to rotate. The stirring bar was driven from outside the tank by another magnetic bar, which was motor-driven. In an earlier design the external driver was a compressed-air-driven magnet, but this did not provide the months of continuous service required. The initial idea was to use air rather than heat-generating motors but by keeping the small (4 W) motor some distance away from the tank, no extraneous effects of heating were noticed. The reliable service of the electrical motor was the more important design consideration.

In addition, each reservoir had an inlet and an outlet line of Tygon tubing to allow the reservoir fluids to be flushed.

The three segments of the tank were assembled in the following way. There is a flange made of 2.54 cm thick Plexiglas on each reservoir, and a matching flange on each end of the test section. After the bottom reservoir is filled with the desired fluid, the porous membrane is stretched over this fluid and held in place as described below. This porous membrane is a sheet of Versapor 800 filter. It has 0.8 micron pore size, and thickness 0.010 cm when stretched. It was stretched under water then held tautly over the reservoir fluid by means of an O-ring which fitted in a groove in the Plexiglas flange. Care was taken, to allow no air bubbles to be trapped under the membrane. In this tautly stretched state, the membrane was flat and rigid. Stirring the fluid on one side of it does not induce flow on the other side. The membrane allows salt and sugar to diffuse through it in accordance with the concentration gradients across it. Fluid flow could be forced through it but we always took precautions in these experiments to ensure that this would not happen. Thus, when the top reservoir, say, was flushed with fluid to maintain a desired concentration, the lines to the bottom reservoir were always closed. Likewise, the lines to the top reservoir were closed when the bottom reservoir was flushed. This was the function of the switching mechanism. Further properties of the Versapor filter can be found in Krishnamurti & Zhu (1989).

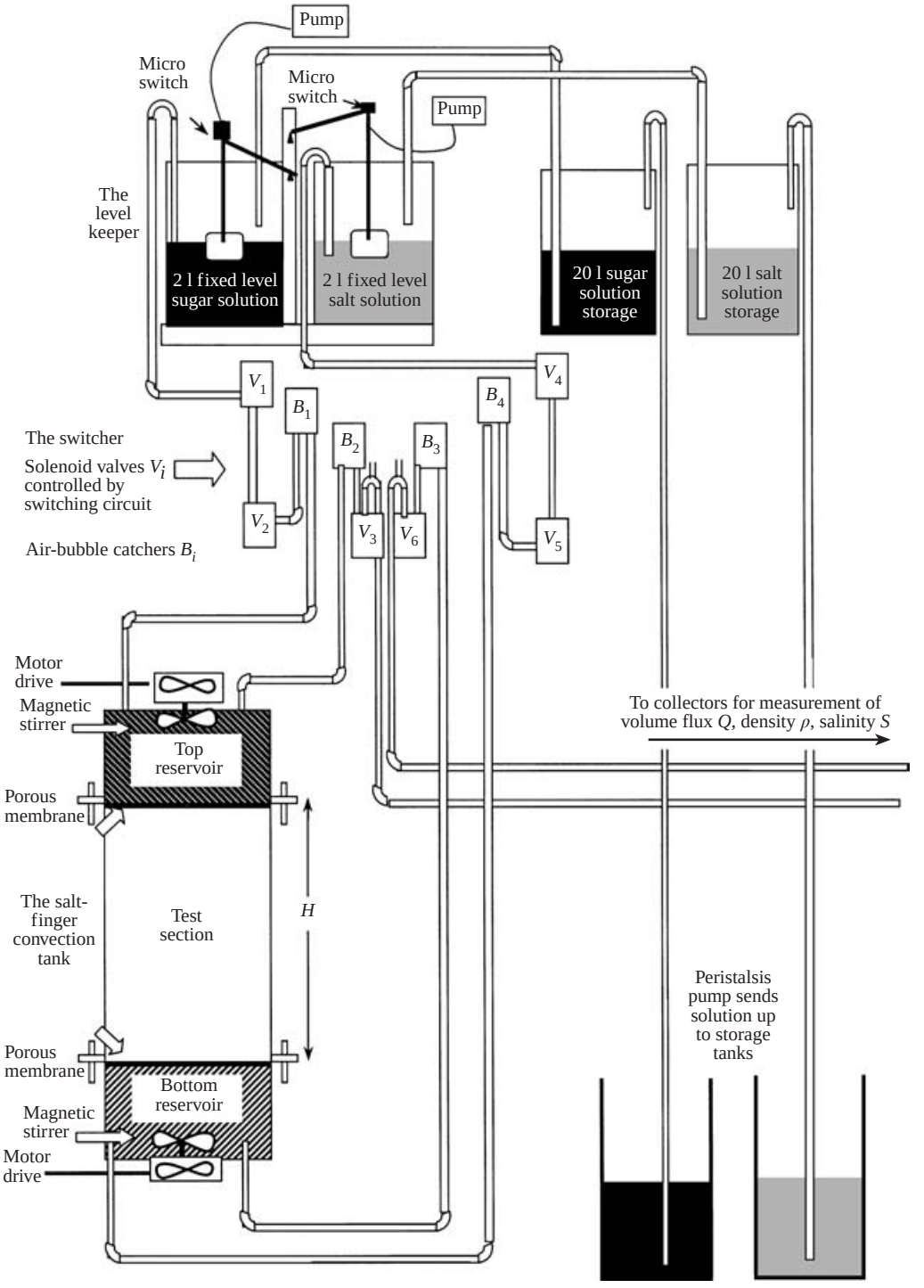

FIGURE 2. Schematic diagram of the apparatus.

With the membrane tautly in place, another O-ring was set in its groove in the flange (just outside the one holding the membrane). The function of this O-ring was to provide the seal when the two matching flanges were bolted together with 48 bolts.

Now, with the test section in place, it could be filled by the procedure described below. Then another stretched Versapor filter was placed on top of this fluid, held tautly in place by another O-ring in its groove, the sealer O-ring was set in place, the top reservoir placed over this, and the two flanges bolted together with a further 48 bolts.

Figure 2 also shows the level keeper and the switcher which together controlled the flushing of reservoirs. The switcher was an electronic controller that opened and closed the solenoid valves, labelled $V_1 \ldots V_6$. It was set to operate as follows: with V_1, V_2, V_3 closed, V_4, V_5, V_6 were opened to allow the flushing of the bottom reservoir with salt solution for a duration of 15 minutes. Then V_4, V_5, V_6 were closed, and, after a short delay of some seconds, V_1, V_2, V_3 were opened, and the top reservoir was flushed with sugar solution for a duration of 15 minutes. This cycle was repeated for the duration of the experiment. The flow rate or volume flux Q through the reservoirs was controlled by the hydrostatic head at the source of the sugar and salt solutions, and by a capillary dripper. This head was maintained constant by a float which, via a microswitch, would activate a pump to add solution to the source from the storage tank if the float level dropped. The capillary dripper was made by heating and stretching a glass tube. The resulting capillary was cut away until the desired flow rate was achieved. The outflow from the flushing was collected, the volume flux Q recorded, its specific gravity and conductivity measured and recorded. A specific gravity balance gave measurements to five significant figures (four decimal places). A portable laboratory salinometer gave conductivity to five significant figures. Where three significant figures were sufficient, we used a simpler immersion-probe-type conductivity meter.

Although this switching system worked for durations of weeks, the solenoid valves would ultimately fail from the salt solution attacking their metal parts. After many dozens of solenoid valve replacements, an alternative mechanical switcher was used in some of the experiments. This consisted of a Teflon valve operated by a synchronous motor. This valve consisted of a shaft rotating in a snug-fitting sleeve. The shaft had flow-through holes for the sugar solution oriented at right-angles to the flow-through holes for the salt solution. At one orientation of the shaft, sugar solution from tubes in the sleeve match the flow-through holes, allowing flow into and out of the top reservoir. At 90° rotation of the shaft, the other tubes in the sleeve match the flow-through holes for salt solution to and from the bottom reservoir. Because of the tight-fitting construction, a high-torque 3 r.p.h. motor was used to drive this valve. In construction, the rotatable shaft was chilled in liquid nitrogen to allow easy assembly, as any small burr or sharp edge, if forced in, could scratch the surfaces and lead to leakage.

The various methods of flow visualization and internal field measurements required several kinds of apparatus.

(*a*) Shadowgraphs: To make shadowgraphs of salt fingers 183 cm tall and a few millimetres wide, we constructed a 'camera' which housed the three tanks. The tallest tank, with reservoir and stirring mechanisms, stood 3 m tall. Thus the 'camera' was made 3.3 m tall, and was 2.4 m by 1.5 m in horizontal dimension. It was made light-tight and painted a flat black inside. In total darkness, photographic paper of length 2 m and width 28 cm could be hung on a wall, or at some desired distance l_2 from the tank, or even on the tank itself. Light from a 2 W zirconium arc lamp with arc size just 1 mm and approximating a point, distance l_1 from the arc to the tank ($l_1 < 2.4$ m), was allowed to pass through the working section of the tank and onto

the photographic paper. Salt fingers produce density and refractive index variations in the working fluid, which then acts as the 'camera lens', focusing the incoming beam of light to produce the shadowgraph. The exposed paper could be processed as usual to make photographic prints.

(*b*) Particle tracking velocimetry (PTV): A camera using 10 cm by 12.5 cm photographic film was multiply exposed to make PTV photographs of tracer particles in the fluid, illuminated by a sheet of light from a 25 mW laser. The exposure protocol is described below in § 3.

(*c*) Particle image velocimetry (PIV): A high-resolution digital camera was used to record and follow the positions of clouds of tracer particles, illuminated by a sheet of light from a 25 mW laser. These images could be analysed to give instantaneous horizontal and vertical velocity components as functions of position. The method of analysis is described below in § 3.

(*d*) Measurements of $\overline{T}(z)$ and $\overline{S}(z)$: Horizontally averaged sugar concentration $\overline{S}(z)$ as it varies with vertical coordinate z could be determined by measuring the optical rotation of a sheet of polarized laser light. The refractive index $\eta(z)$ could be determined from the angle of deviation of a laser beam. The apparatus for these measurements consisted of two lasers and rotatable Polaroid films all riding up or down on a vertical trolley. The laser for determination of $\eta(z)$ was attached to a circular vernier scale for accurate angle measurement.

2.1. *Materials used*

In preparing the solutions, we did not use laboratory grade but rather food grade cane sugar and kosher salt from the grocery store as the cost of the former, for the large quantities needed, would have been prohibitive. Approximately a ton of salt and 1.5 tons of sugar were consumed for these experiments. Kosher salt was used as it is free of calcium silicate often found in table salt; the former makes clear solutions while the latter does not. Also, many thousands of litres of distilled water were used to prepare the solutions for filling the tanks and flushing the reservoirs.

For the higher-salinity experiments it was necessary to boil the distilled water to de-gas it. Although adding salt de-gasses the water of the salt solution, when this comes into contact with the sugar solution in the fingering experiments, the salt tends to de-gas the sugar solution if it has not been previously de-gassed in its preparation, and bubbles form on the container walls. In addition, a few grams of sodium fluoride were added to 20 litres of sugar solution, in order to retard the growth of micro-organisms.

For PIV and PTV photography, the tracer particles were silver-coated hollow glass spheres with diameters in the range of 8 to 20 microns. These were separated in a settling tank to collect only those nearly neutrally buoyant at the average fluid density of the particular experiment. For the PTV photography, 60 mm negative film was used. For recording the shadowgraphs, Kodak polycontrast II RC paper was used, in 27.9 cm $\times$ 152 m rolls. Approximately 300 m of this paper was used for the shadowgraphs.

3. Procedure

The sugar and the salt solutions were prepared with the de-gassed distilled water. The bottom reservoir was filled with the salt solution, the porous membrane stretched into place, then the test section was bolted on. The test section was filled with opposing

vertical gradients of sugar and salt, using the two-bucket method. Two identically sized holding tanks, one for the sugar solution, the other for the salt solution, were placed on the roof of the camera, and equal volumes of each solution were pumped up to the roof. A total volume of 55 l was needed to fill the largest test section. The two holding tanks were connected with a siphon so that their fluid heights would remain equal. The sugar solution was then gravity-fed into the test section through an inlet tube near the bottom of the section. Since this would lead to salt solution siphoning into the sugar holding tank, the latter was constantly stirred with a magnetic stirring bar. As the salt solution was more dense than the sugar solution, later-entering fluid would lie below earlier-entering fluid in the test section. The flow rate was slowed to produce a filling rate of 5 cm depth per hour. We varyied this rate by as much as 50%, without a visible difference in the resulting stratification. Thus a nominal rate of filling of 5 cm per hour was used. At this rate it takes approximately 2 days to fill the largest tank. Also at this rate, early-formed fingers or other flow structures are lifted up so slowly that no visible disruption is noticeable. In order to avoid any jet-like flow from the inlet tube, a small flat disk of Plexiglas was fixed at right angles to the inflow direction, 5 mm inside the tank so that the entering flow would be diverged and inflow speed reduced.

When the test-section filling was completed, the top porous membrane was stretched into place and the top reservoir bolted on. Then the top reservoir was filled with the sugar solution, and the flushing of the two reservoirs was started. Each reservoir was constantly stirred even during the non-flushing phases. The reservoir T and S values could be held fixed by means of this flushing, or the flushing could be turned off and the system allowed to run down as in the classical Turner experiments. In the latter case, the run-down time was typically on the order of a month. Throughout this time, the reservoir stirring was always maintained. In this run-down mode, fluid samples were extracted from the reservoirs at fixed time intervals, T and S measured, then the sample was returned to the reservoir with very little loss of volume.

Early in the experiment series, data of many forms (including time-lapse photography of shadowgraphs) was frequently collected to learn the nature of the flow and its variability. However, after many trials the following routine was found sufficient.

Once per day, the accumulated output of the flushing was collected and analysed for conductivity c and density ρ. In the run-down mode, reservoir fluid was extracted, measured, then returned to the reservoir, once per day. Also once per day, a shadowgraph photo was exposed, followed immediately by a vertical scanning to determine the optical rotation angle $\phi(z)$ and refractive index $\eta(z)$. A series of calibration measurements was made so that from any pair of measurements (c, ρ) the salt concentration and the sugar concentration of the reservoirs could be determined. For the internal measurements of $\phi(z)$ and $\eta(z)$, the equations of Ruddick & Shirtcliffe (1979) were used to infer the sugar concentration $w_S(z)$ and the salt concentration $w_T(z)$.

PIV and PTV were not done routinely, but only occasionally to find the relationship between these and the shadowgraph images.

4. Observations

4.1. *Flow visualization*

4.1.1. *Shadowgraphs*

Excerpts from typical shadowgraphs are shown in figures 3–7. These were directly exposed and recorded on photographic paper of width 28 cm and various lengths cut

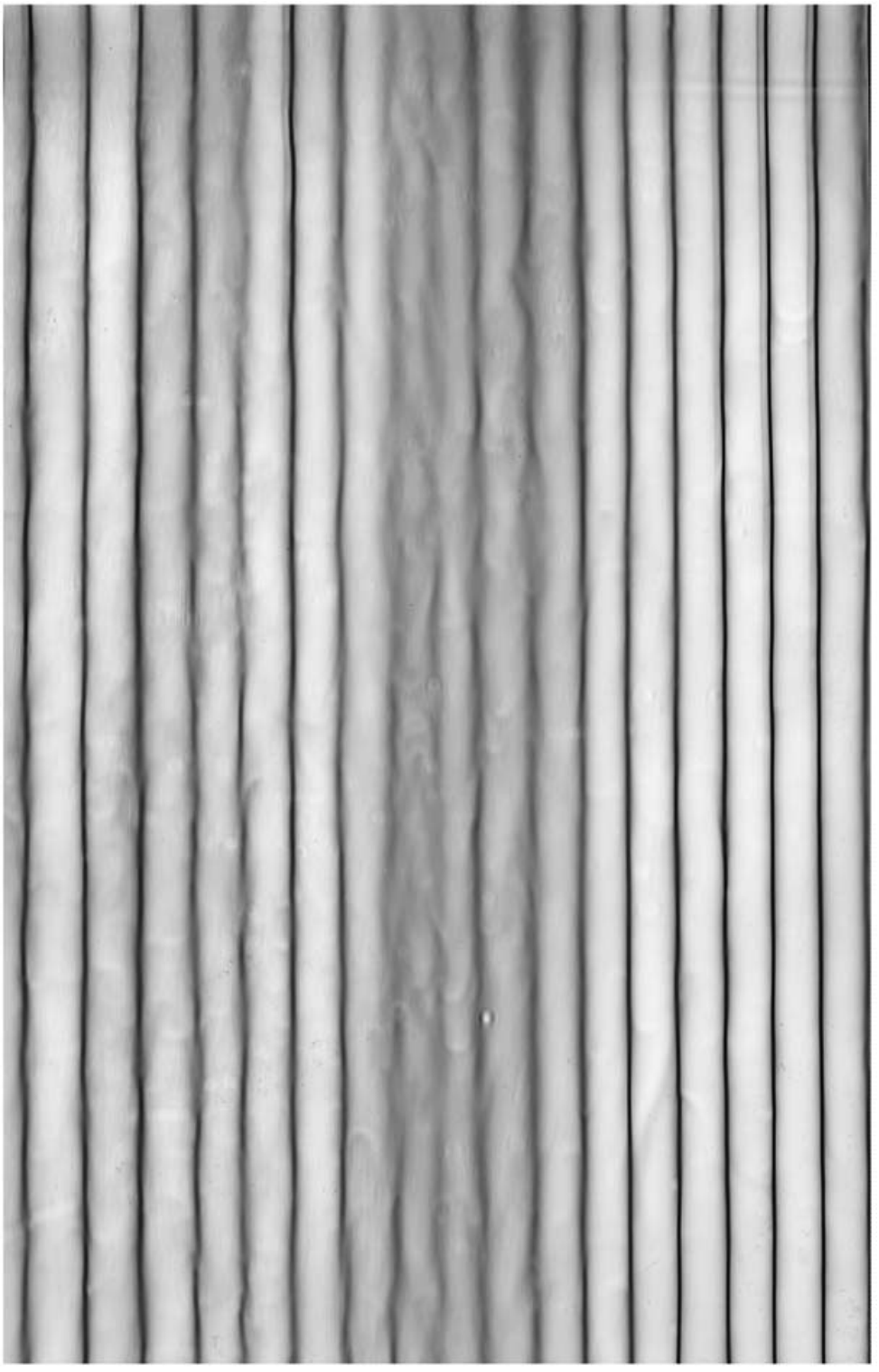

FIGURE 3. Shadowgraph of straight salt fingers. The part shown here is an excerpt from a 2 m tall shadowgraph of straight fingers. The width of the image corresponds to 6.0 cm at the tank. Exposure time was 6 s. $|R_S| = 7.12 \times 10^{15}$, $R_\rho = 1.25$, Stern number $\mathscr{A} = 0.20$.

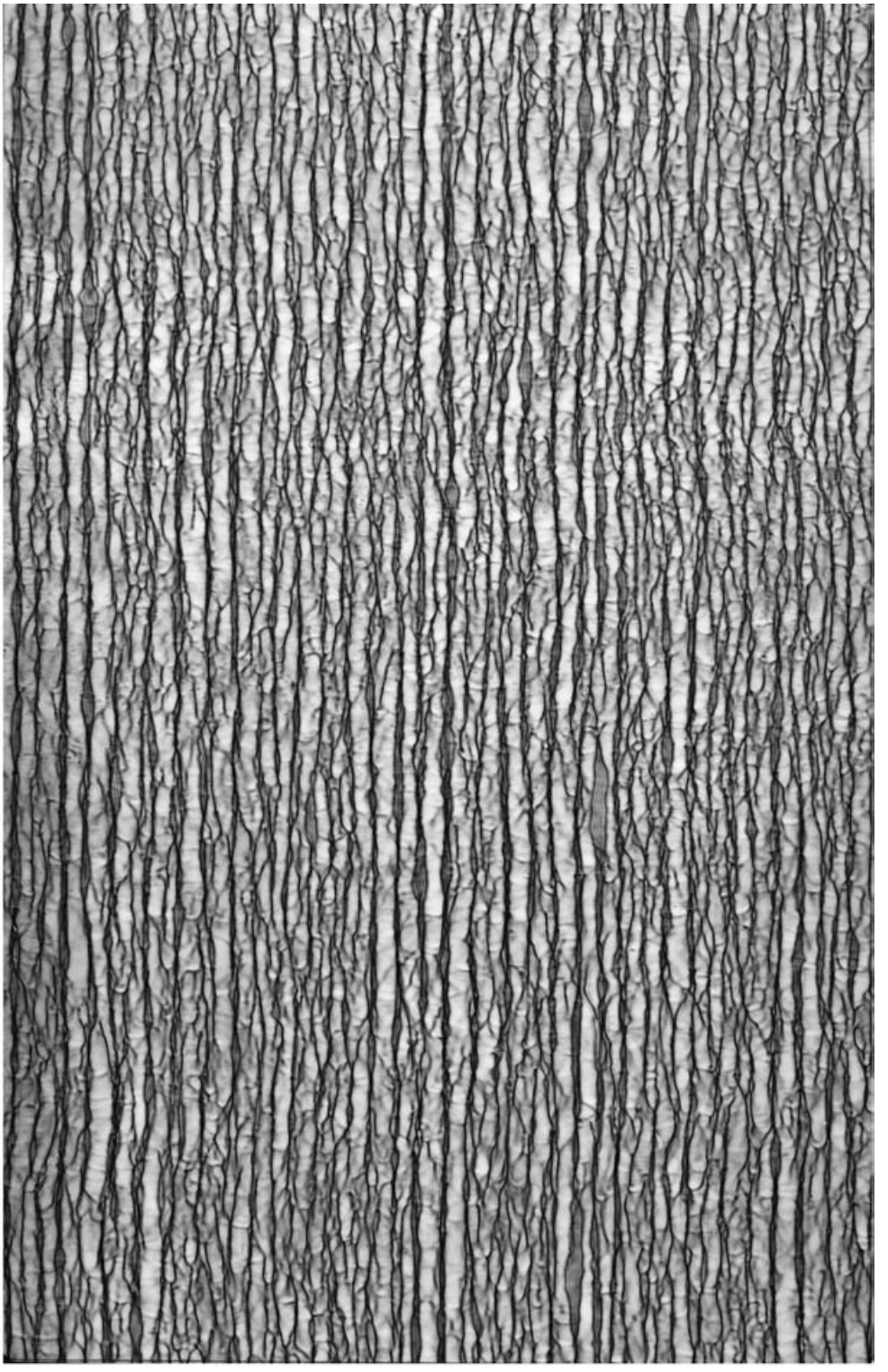

FIGURE 4. Shadowgraph of lumpy salt fingers. The part shown here is an excerpt from a 2 m tall shadowgraph of lumpy fingers. The width of the image corresponds to 8.5 cm at the tank. Exposure time was 10 s. $|R_S| = 7.60 \times 10^{15}$, $R_\rho = 1.25$, $\mathscr{A} = 0.39$.

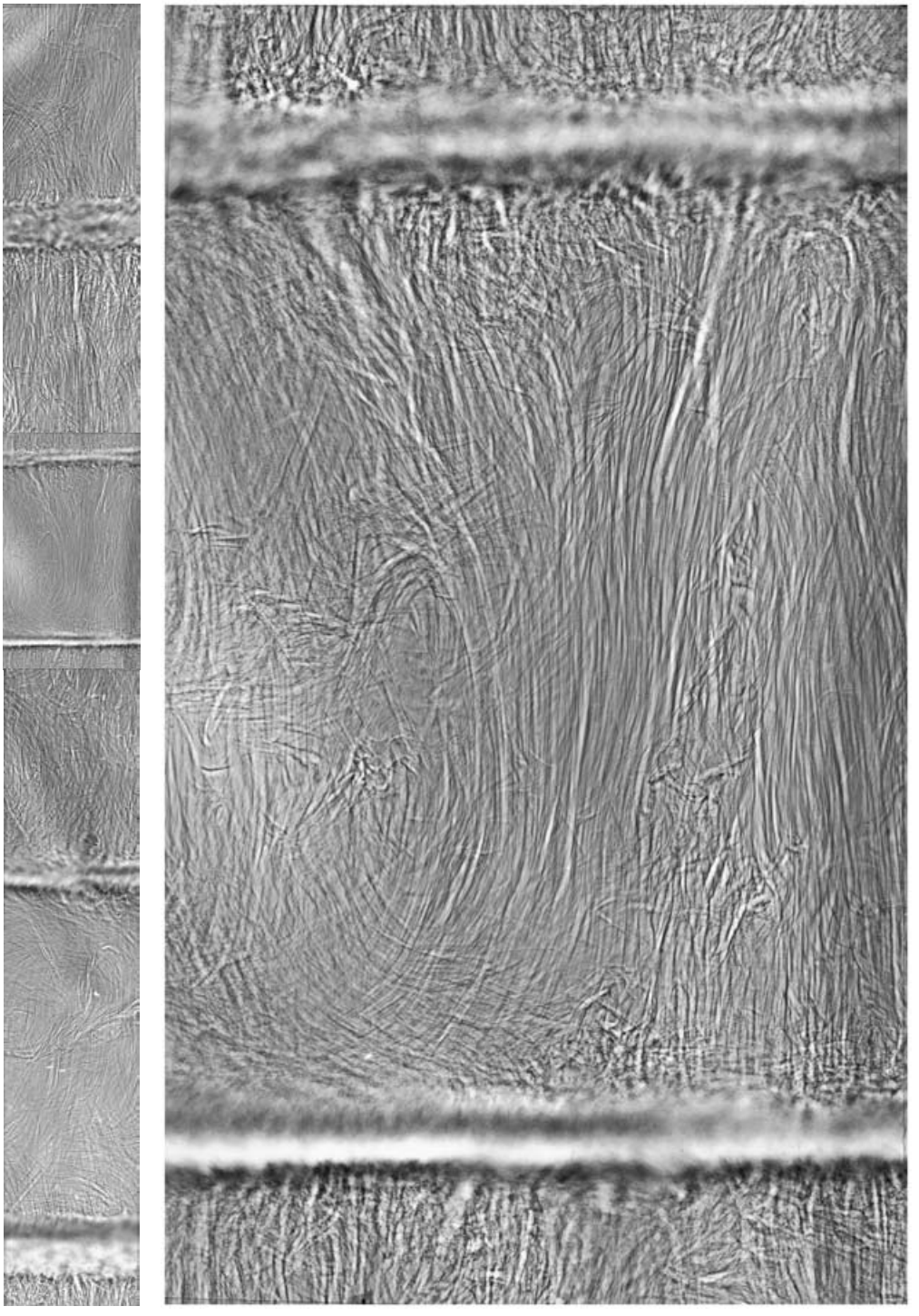

FIGURE 5. For caption see facing page.

as needed. The magnification m of the image is $(l_1 + l_2)/l_1$, where l_1 is the distance from light source to front plane of the tank, l_2 the distance from back plane of the tank to the plane of the photographic paper. (The tank dimension in the direction of the optic axis is 10 cm.) The values of m used vary from approximately 1 to 6, and these values are known for each photograph. However, as further magnification may occur in reproduction, the actual dimension at the tank is given with each photograph. When the photographic paper is attached directly to the back plane of the tank, $l_2 = 0$ and $m = 1$. Exposure times were typically 5 to 10 s, which was fast enough to capture most flows encountered.

As so many fascinating shapes of flows were encountered as $(\Delta S, \Delta T)$ were varied, we made frequent recordings. These were roughly categorized into the four types shown in figures 3, 4, 5, and 7. These are all from the 2 m tank with ΔS, ΔT maintained by flushing reservoirs. They are categorized by salt Rayleigh number R_S, density ratio $R_\rho = \alpha \Delta T / \beta \Delta S$, and where relevant, the Stern number $\mathscr{A} = F_S/(\nu\alpha\partial\bar{T}/\partial z)$ (Stern 1969), where F_S is the salt flux. Figure 3 shows straight fingers. Although only 20 cm of length is shown, there is no detectable difference with any other excerpt taken from along the 2 m length. Figure 4 shows irregularities or 'lumpiness' on the fingers, giving an appearance of tree bark. Time-lapse photography shows these lumps to travel up or down on alternating fingers with an apparent speed on the order of 10^{-2} to 10^{-3} cm s^{-1}. Many variations can be found in this general category. Again, this 20 cm excerpt from the 2 m length looks indistinguishable from any other 20 cm excerpt. Figures 3 and 4 might be called vertically homogeneous over the 2 m, and on scales greater than 10 cm. Figure 5 shows a differentiation into a staircase of alternating finger layers and convecting layers. Figure 5 is an excerpt from a 2 m vertical length that had ten finger layers and nine convecting layers. The narrow strip at the left shows six of the ten finger layers. To the right of this narrow strip is a magnified view of two (blurred) finger layers and one convecting layer. The blur is due to the rapid fluctuations at the junction of the finger and convecting layers. When the finger layer has increased in depth, as in figure 6, this junction is less blurred. Figure 7 shows the whole field of fingers organized into wavy forms.

Clearly, each of these categories may be studied to determine what controls the variations. For example, with straight fingers (figure 3) we often see a group of sharp fingers interspersed in the horizontal direction with a group of fuzzy fingers. This phenomenon is not addressed in this paper. The many forms of tree-bark patterns are also not addressed here. The waves of figure 7 and their evolution will be treated in a separate paper. Here we consider only the staircase as depicted in figure 5 and 6.

The interpretation of these shadowgraphs is clarified in several ways. First, we solved numerically the perturbation eikonal equation, then the ray equation, to find the path of an initially parallel beam of light travelling in the y-direction that enters a field of salt fingers uniformly arranged in the horizontal (x, y)-plane, then emerges

FIGURE 5. Shadowgraph of a portion of a thermohaline staircase. This excerpt is from a 2 m tall shadowgraph which had ten finger zones and nine convection zones in alternation. The narrow strip at the left corresponds to 101 cm out of the total 183 cm depth of the tank and shows six finger zones and five convection zones. Due to limitations of the scanner, the shadowgraph is spliced in the third convection zone. Shown on the right is a blow-up of the third full convection zone bounded by two (blurred) finger zones. The blurring is from rapid fluctuations at the junction between finger and convection zones. The height of the image to the right corresponds to 16 cm at the tank. Exposure time was 10 s. $|R_S| = 1.00 \times 10^{16}$, $R_\rho = 1.25$.

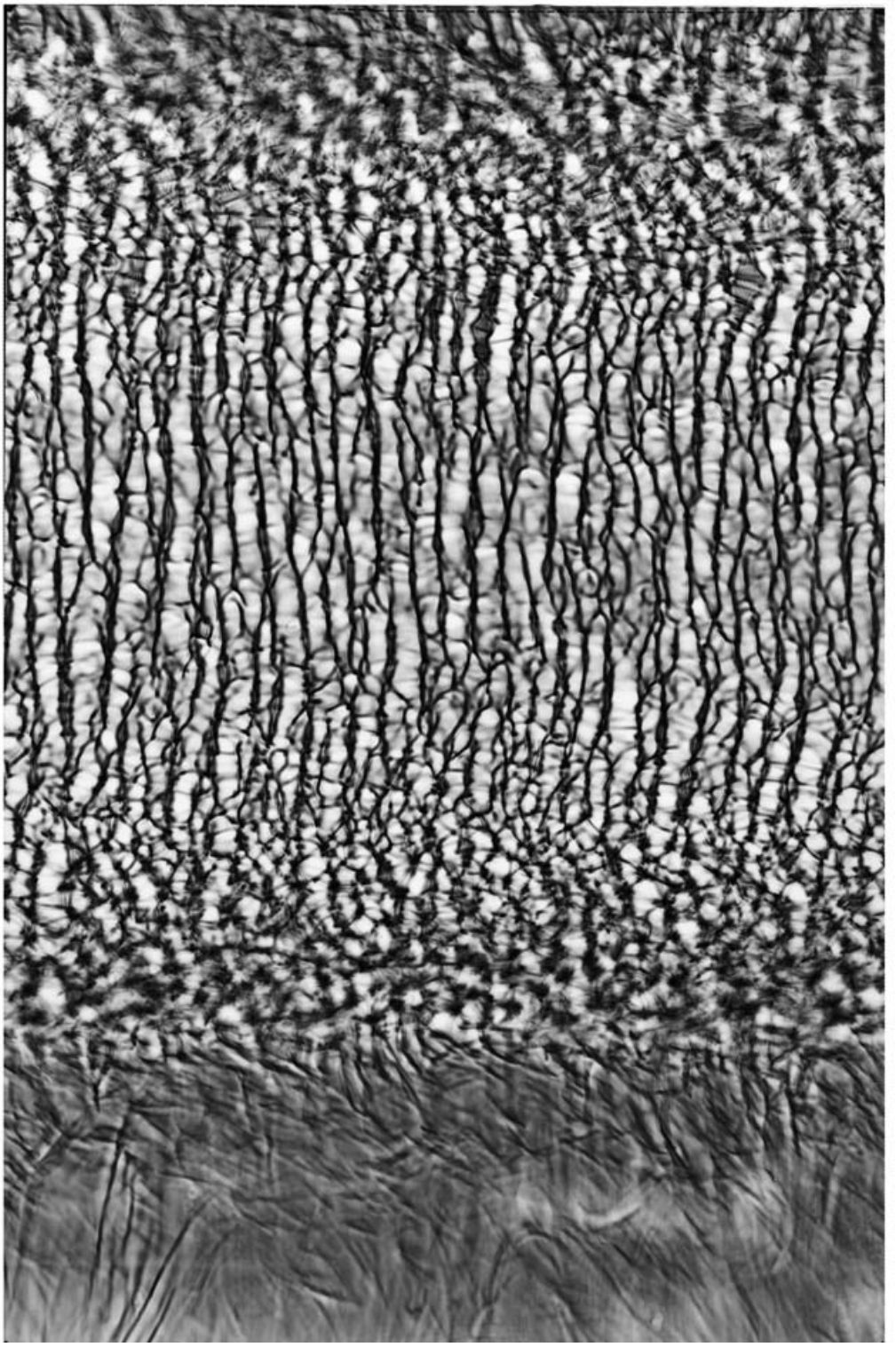

FIGURE 6. Shadowgraph of a portion of a thermohaline staircase showing a magnified view of a finger zone. The width of this image corresponds to 13.6 cm at the tank. Exposure time was 10 s. $|R_S| = 9.42 \times 10^{15}$, $R_\rho = 1.25$.

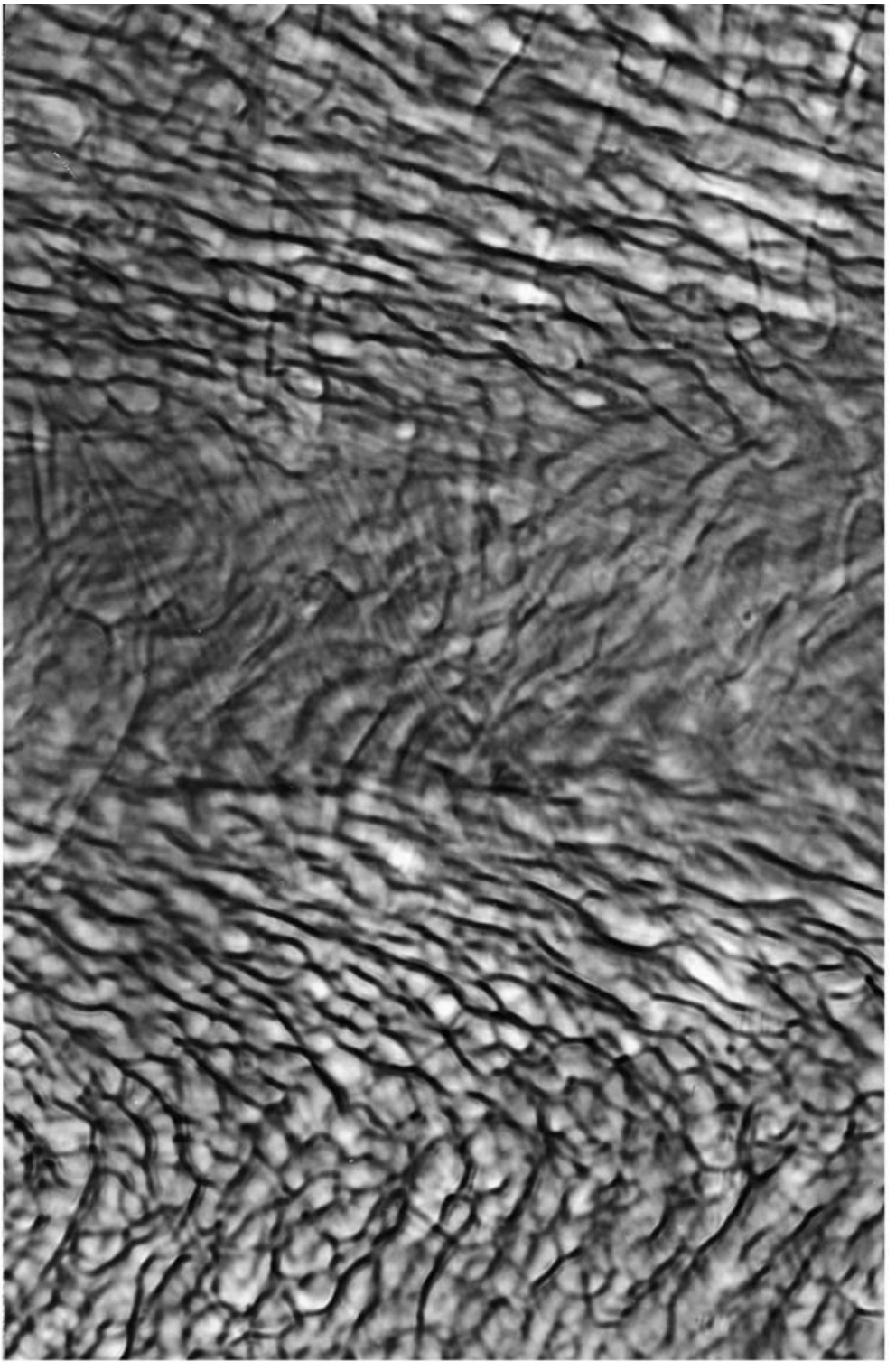

FIGURE 7. Shadowgraph of wavy salt fingers. The width of the image corresponds to 10.30 cm. Exposure time was 10 s.

to be focused on some focal plane. This study will be reported elsewhere. The idea is the same as the Shirtcliffe & Turner (1970) interpretation of a shadowgraph that might be produced by a single row of fingers, where higher-refractive-index fingers act as converging cylinder lenses.

The interpretation of these shadowgraphs is further clarified by a view of the flow in the vertical (x, z)-plane, not averaged in y, as produced for PIV and PTV.

4.1.2. *PTV and PIV images*

Figure 8 shows salt fingers and convection in a portion of a thermohaline staircase. Figure 8(a) shows the shadowgraph in the (x, z)-plane and y-averaged. Figures 8(b) and 8(c) are PTV images showing the same region, in the (x, z)-plane at mid-tank, $y = 1/2$. Figure 8(d) shows the velocity field in the same region using PIV Sleuth (Christiansen, Soloff & Adrian 2001). All four views were taken within minutes of each other.

For the PTV image of figure 8(b), the protocol used was 10 s light, 20 s dark, repeated five times; then 30 s dark; then 10 s light, 20 s dark, repeated three times. This would lead to five bright spots from each reflecting particle, followed by a dark 'spot', then followed by three bright spots. The asymmetrical placement of the dark 'spot' gives the direction of the particle motion, while the spacing of the bright spots on the film gives the speed. Because of the great variation in speed within the convective flows, when using this protocol the motion is hard to distinguish. Nevertheless, the swirling flows of the convection can be easily seen. In the region below this convection, the tracer particles appear stationary. However, for the PTV image of figure 8(c), taken immediately after 8(b), the protocol used was 30 s light, 60 s dark, repeated five times; then 90 s dark; then 30 s light, 60 s dark, repeated three times. Now the up-and-down motion in the fingers becomes apparent, although the convective flow is blurred.

4.2. *Flux measurements*

As mentioned in the introduction, the same contrast $(\Delta S, \Delta T)$ between top and bottom reservoirs, with initially linear gradients in the test section, did not result in the same flux F_S in the three tanks of depths 2 m, 1 m, and 0.3 m. The 0.3 m depth had the largest flux, then the 1 m depth; the 2 m depth had the smallest of the three values of F_S, even though the 2 m tank obviously has the largest Rayleigh number.

In these comparison experiments, it was noted in the shadowgraph that the 0.3 m tank had salt fingers extending from top to bottom reservoirs, whereas the 1 m tank had three finger interfaces and two convection zones. The 2 m tank had six finger interfaces and five convection zones. This layered system, say of six finger zones alternating with five convection zones, could be maintained indefinitely by maintaining ΔS and ΔT with reservoir flushing. This number of layers is usually smaller than that formed initially, but some steady number is reached in the flushed system. If the reservoirs were not flushed, finger layers would always grow in height on a time scale of days, ultimately merging with other finger layers as the convecting layer between disappeared. The reverse process of finger layers breaking apart and forming a convecting layer was never observed on these long time scales.

The following data are for such a run-down in the 1 m test section. The initial state, produced by the two-bucket method, was a salt profile linear between ΔSa at the bottom reservoir and zero at the top, along with a sugar profile linear between zero at the bottom and ΔSu at the top. This profile broke down to form eight finger layers and seven convection layers. The breakdown occurred even as the tank was being

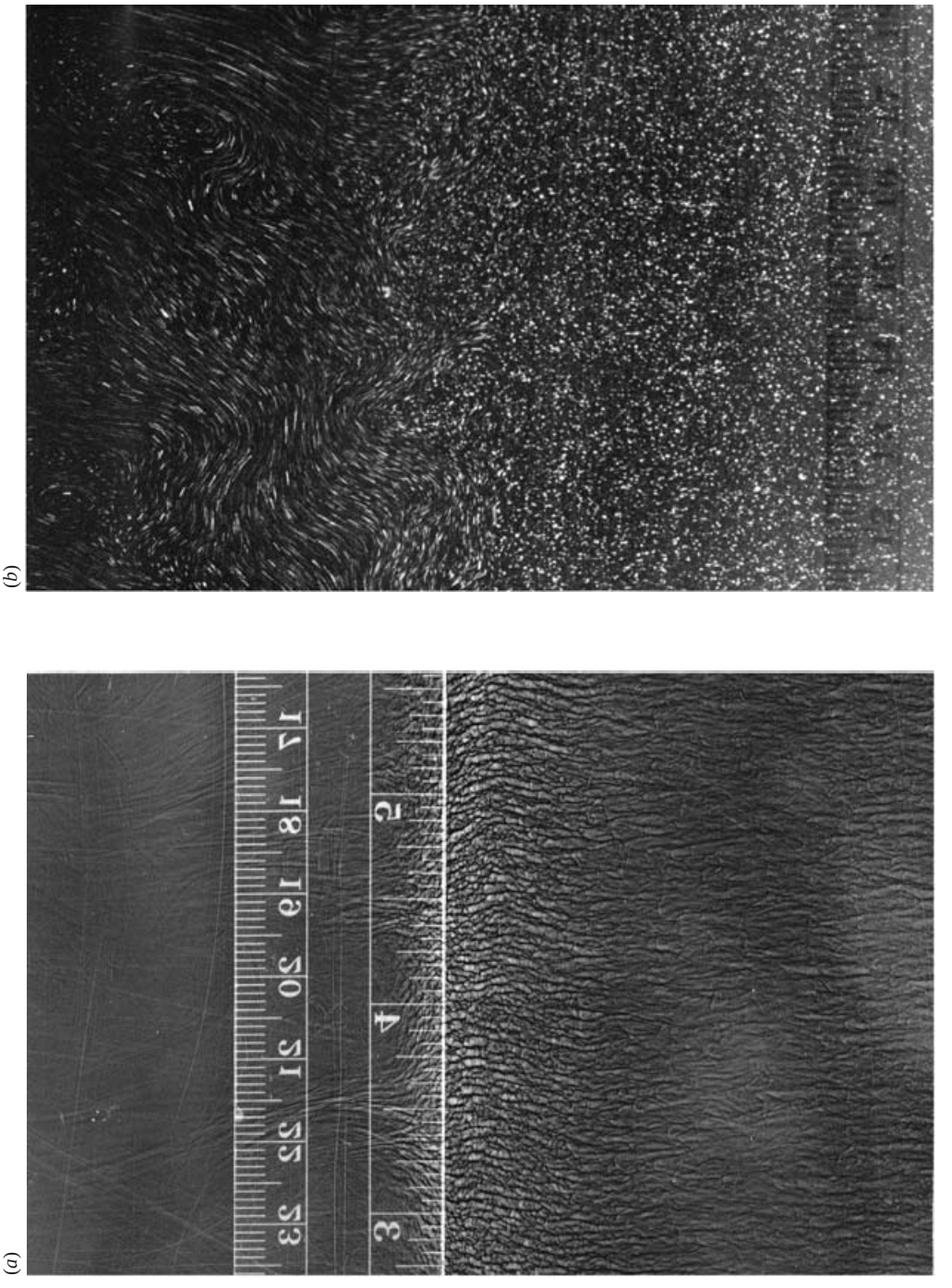

FIGURE 8(*a*,*b*). For caption see page 305.

FIGURE 8. For caption see facing page.

filled. Altering the filling rate (20 hours to fill versus 30 hours to fill) or the filling method (filling from below versus filling from above onto a floating sponge) did not alter the eight/seven layering. This could be altered only by changing ΔSu and ΔSa, that is, by changing the initial gradients.

For a month, measurements (i.e. shadowgraph, refractive index $\eta(z)$, optical rotation $\phi(z)$, as well as flux measurements in the reservoirs) were taken daily and both reservoirs were continually stirred but not flushed. During this period the general trend was for finger interfaces to grow thicker and convection zones to shrink in height. Sometimes a convection zone vanished totally and the two neighbouring finger zones merged. These mergers of finger zones usually occurred in a time period of a day or less, although the impending merger could be anticipated for some days prior. In the days following the merger, the reservoir fluxes vacillated. These are seen as the spread in N_S in figure 9 at one value of the number n of interfaces. This number n is not a good independent variable, but perhaps serves to show the strong relationship between F_S, N_S, and the number of layers. After approximately 20 days, the number of finger interfaces had decreased to one; that is, fingers extended from top to bottom reservoirs without convection zones. Figure 9 shows the Nusselt numbers N_S and N_T as they changed with the number of interfaces. The filled circles and the broken line show the sugar Nusselt number N_S; the open symbols (squares, circles, triangles, and crosses) show the salt Nusselt number N_T. The labels $\frac{2}{3}R$ and $\frac{1}{2}R$ indicate that the initial values of ΔS and ΔT were each reduced to $\frac{2}{3}$ of the value for the curves labelled R in the one case, and to $\frac{1}{2}$ of that value in the other case. The density ratio R_ρ was initially the same at $R_\rho = 1.17$ for all these experiments. N_S and N_T follow each other exactly for the first 8 days, then diverge, as described below.

In many repetitions of these experiments of run-down from an initial gradient, we always found that for the first 5 to 10 days (when there were five to ten finger interfaces), the export of sugar out of and the import of salt into the top reservoir compensated each other: the density ρ of the top reservoir remained unchanged to the fourth decimal place, even though the salinity was constantly increasing. We therefore infer that the sugar concentration was constantly decreasing. This is shown in figure 10. We defined

$$\sigma = (\rho - 1.1695) \times 10^4$$

to show small deviations in density ρ. Also plotted are αSa where Sa is measured salinity and $\alpha = 6.12 \times 10^{-4}$(g l^{-1}), and βSu which is inferred from the density and salinity, with $\beta = 3.26 \times 10^{-4}$(g l^{-1}). This observed constancy of ρ while the Sa concentration increases and the Su concentration decreases appears to be related to

FIGURE 8. Four different views of one region of a thermohaline staircase, showing fingers and convection. (*a*) A shadowgraph with fingers below the ruler, convection above the ruler. The light beam averages in the y-direction. The area shown is 7.3 cm wide by 11 cm tall. (*b*) A photograph prepared for PTV of the same region, showing convective flow in the upper 40% of this (x, z) view at y mid-distance in the tank. The fingers in the lower half appear as stationary fluid. The ruler has been moved down from its position in (*a*). Duration of this photograph was 270 s. (See text for exposure protocol.) The area shown is 7.3 cm wide by 11 cm tall. (*c*) As in (*b*), except that the duration of the photograph was 810 s. (See text for exposure protocol.) The ruler is in the same place as in (*b*) but we show a lower portion of a large photograph. The area shown is 7.3 cm wide by 11 cm tall. With this longer exposure, the vertical motion in the fingers becomes apparent. (*d*) A PIV-derived velocity field showing velocity vectors in the convection zone. The area shown is 11 cm wide by 8.5 cm tall.

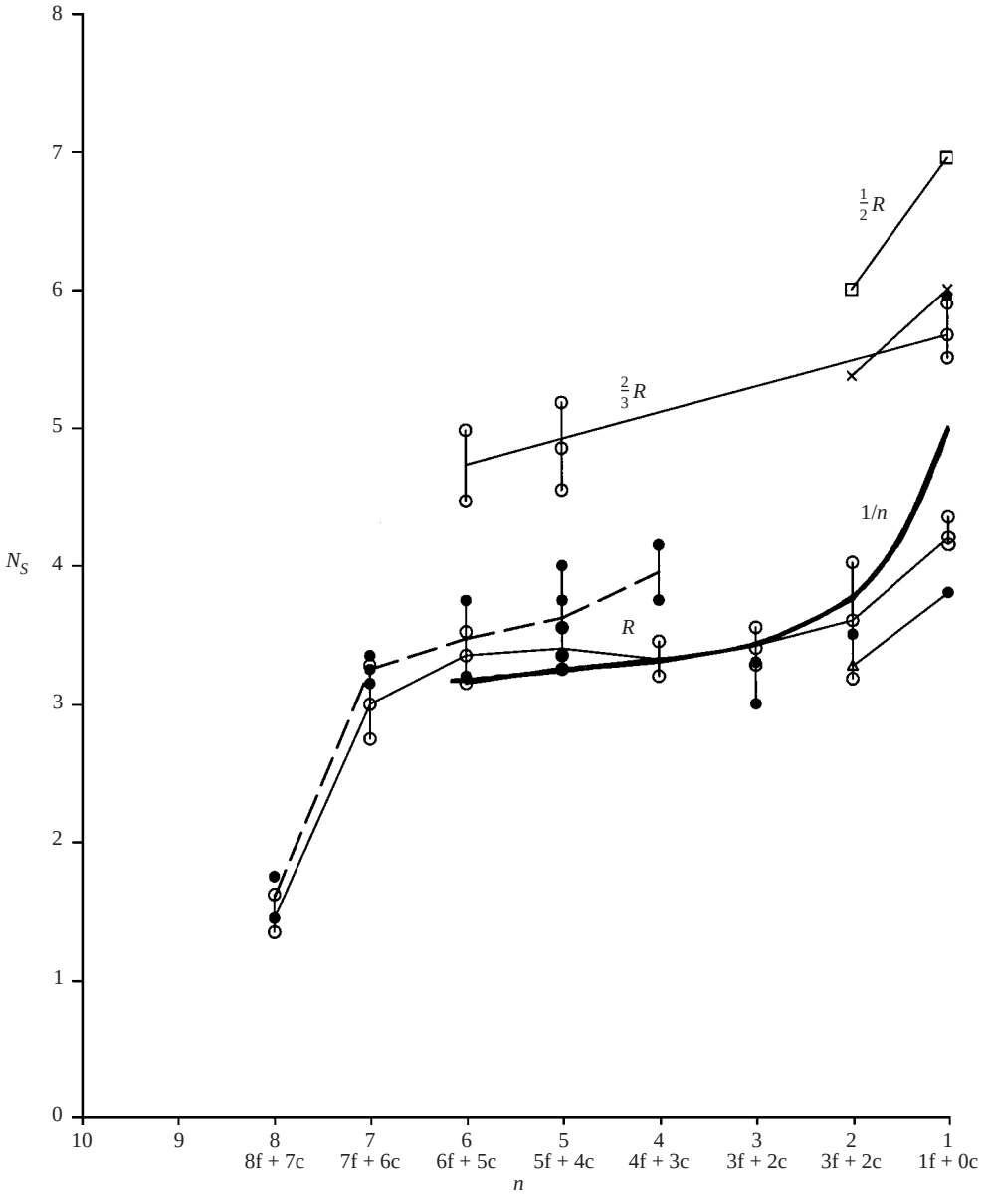

FIGURE 9. The variation of the overall Nusselt number N_S with the number n of finger layers in the 1 m tall tank. The labels R, $\frac{2}{3}R$ and $\frac{1}{2}R$ refer to relative initial concentration gradients of 1, $\frac{2}{3}$, and $\frac{1}{2}$ for S and T. $R_\rho = 1.17$ for all these experiments. The filled circles and the broken line are for the sugar Nusselt number N_S; the open symbols are for the salt Nusselt number N_T. For both Nusselt numbers $C = 0.304$. N_S and N_T always follow each other precisely for the first 5 to 10 days, in the sense of figure 10. The heavy solid curve represents a function $N \sim 1/n$. Along the abscissa, under $n = 8$ for example, the notation 8f + 7c indicates eight finger layers and seven convection layers.

a chemical bond theory of density of salt solutions (Dougherty 2001), but why it first holds at dilute concentrations of *Sa*, then fails after some time in our experiments is unclear.

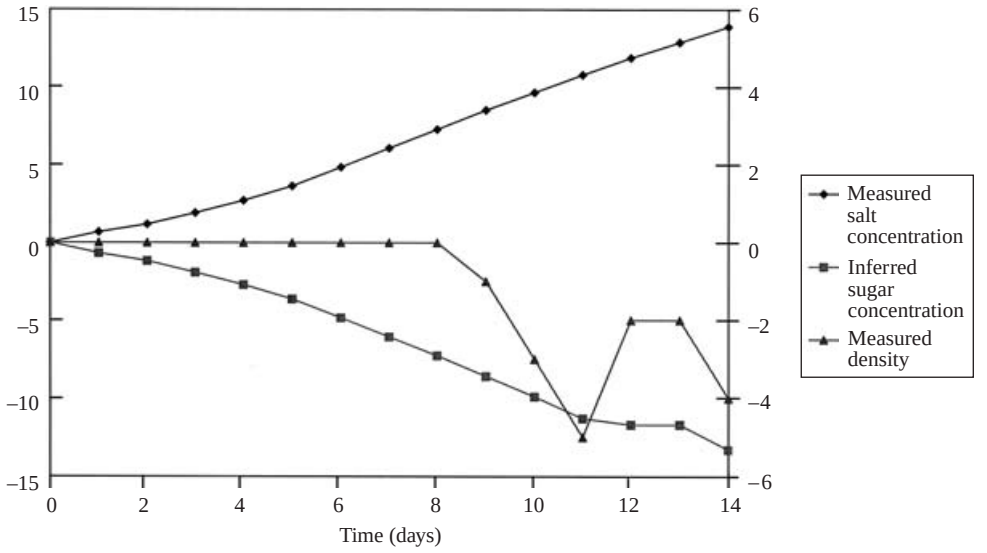

FIGURE 10. The measured density ρ, expressed as $\sigma = (\rho - 1.1695) \times 10^4$ (right-hand axis); the measured salinity Sa expressed as change in density anomaly αSa; and the inferred sugar concentration, expressed as change in density anomaly βSu (left-hand axis).

4.3. *Internal measurements*

The data $\eta(z)$ and $\phi(z)$ were converted to weight fractions $w_S(z)$ and $w_T(z)$ using equations from Ruddick & Shirtcliffe (1979). Our data had the following characteristics. Each convection layer was well-mixed upon horizontal averaging, with η and ϕ constant in z. The junction between the convection layer and the finger layer fluctuated so rapidly that the image of the laser beams made the fluid appear to be 'boiling' and reliable measurements were difficult to obtain here. Early in the experiments, when the finger layers were very short, this boiling appearance dominated the entire finger zone (see figure 5). However, towards the end of the experiment, when the fingers were very long or even filling the tank, both $\eta(z)$ and $\phi(z)$ were smoothly varying linear functions of z within the finger zone, and were easily measured.

Now the main points are the following: the overall stratification is stable, so overall the density Rayleigh number $R = g\{|\Delta w_S| - |\Delta w_T|\}d^3/\kappa_T \nu$ is negative. It must be negative in the finger zones, but between finger layers convective overturning is observed and over most of this layer any local value of R appears to be zero. How and where can one define and reliably measure an internal Rayleigh number which is positive and which characterizes this convective flow?

The observed convection is vigorous, with overturning flow on length scales of tens of centimetres, time scales of minutes, characteristic of flow at large positive Rayleigh numbers and high Prandtl number. This can be seen in figure 8(*b*) where the exposure time was 270 s, as well as in the instantaneous PIV-derived velocity field seen in figure 8(*d*). This convective flow is much faster than flow speeds in the fingers; in the 270 s picture, we see that tracer particles in the finger layer have barely moved. Time exposures increased to 810 s (figure 8*c*) show the motion in the finger layer while the convective motion is blurred.

Figure 11 shows a conceptual model of the staircase stratification. Well-mixed convection layers lead to concentration of the gradients in the finger layers, which then appear to take on the role of boundary layers for the convection. For example,

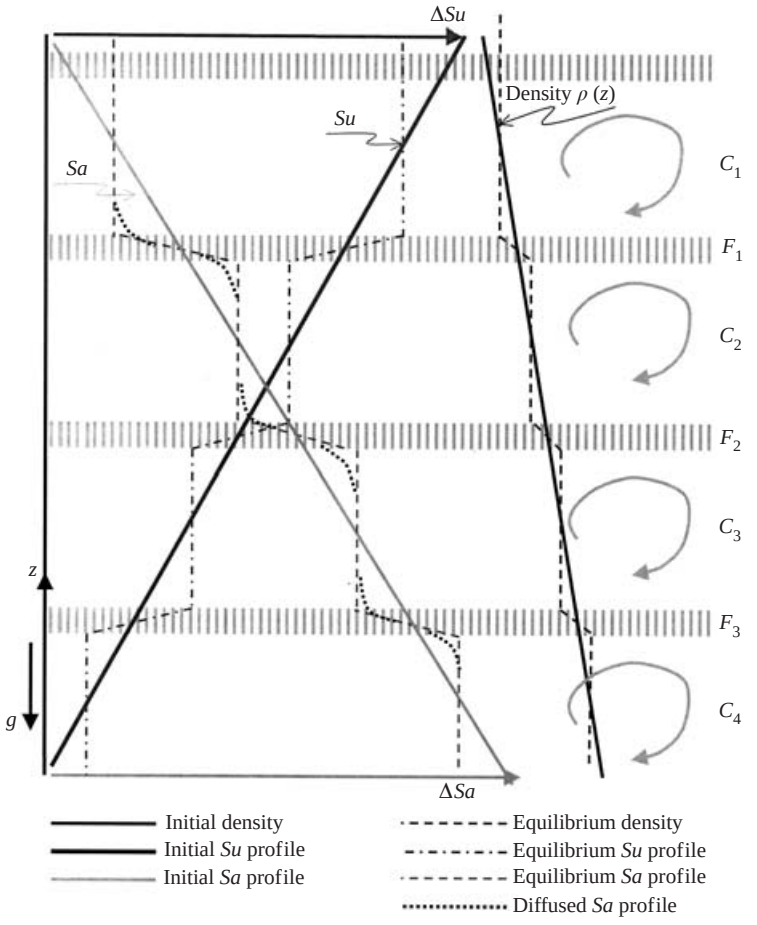

FIGURE 11. A model thermohaline staircase showing the vertical diffusion of salt (T) from the finger interface.

the well-mixed layer C_2 has 'boundary layers' F_1 and F_2, so its total drop in Su (Δw_S) would be the Su value in C_1 less the Su value in C_3. Its total drop in Sa (Δw_T) would be the Sa value in C_3 less the Sa value in C_1. This would still leave $|R_T| > |R_S|$ and $R < 0$. However, allowing Sa to diffuse vertically, while neglecting the diffusion of Su, leads to the dotted profile labelled 'Diffused Sa profile,' which shows the diffusive smoothing of the Sa profile. Now, measuring Δw_T from the Sa value at the edge of C_3 (at the boundary with F_2) less the Sa value at the edge of C_1 (at the boundary with F_1) produces a smaller value of Δw_T. For fingers to persist, the density ratio R_ρ needs only to lie between $1/\tau$ and 1 (where τ is the diffusivity ratio), that is, the density ratio may be relaxed towards one. In fact, at the last measurable data point of η and ϕ before the 'boiling' usually $|\Delta w_S| > |\Delta w_T|$ and $R > 0$. However, this estimate of R would depend upon where in z the measurement was taken. To make this a more uniform estimate, it was decided to use the 'Initial Sa profile' in figure 8 for an estimate of Δw_T, as if Sa had diffused back to the linear profile.

Thus, for the layer C_2, Δw_T is the linear gradient times the distance from the top of F_1 to the bottom of F_2, while Δw_s is the drop from the Su value in C_1 less that

in C_3. We are tapping the *Su* gradient for an effectively deeper layer than for the *Sa* gradient. For the layer F_1, we still used *Sa* in C_2 less *Sa* in C_1 and *Su* in C_2 less *Su* in C_1. We consequently overestimate $|\Delta w_T|$ in F_n and underestimate it in C_n, but consistently for all layers, and not relying on z-estimates and averaging of highly variable quantities. The result is that $R > 0$ in each convection layer and $R < 0$ in each finger layer. The method breaks down when $h_n \gg d_n$, where h is the finger layer height and d is the convection layer depth.

With this framework we expressed the fluxes of *Su* across each finger layer and convection layer as shown below. Then, on the assumption of no flux divergence in these layers, we equated the flux to that measured in the reservoirs. In this way we determined the flux laws described next.

From dimensional analysis, the salt flux $F^f_{S,n}$ across the nth finger layer may be expressed as

$$F^f_{S,n} = \kappa_S \frac{\delta S^f_n}{h_n} f\left(R^{f,n}_S, R^{f,n}_\rho, \tau, Pr\right), \tag{1}$$

where δS^f_n is the salinity drop across the nth finger layer; h_n is the nth finger layer thickness; f is a function of the dimensionless numbers $R^{f,n}_S$, the salt Rayleigh number of the nth finger layer, and $R^{f,n}_\rho$, the density ratio $R^{f,n}_T/R^{f,n}_S$ for the nth finger layer; τ is the diffusivity ratio κ_S/κ_T; Pr is the Prandtl number ν/κ_T.

As τ and Pr are not varied, we express the function f as a function of $R^{f,n}_S$ and $R^{f,n}_\rho$ only, writing this as a power law:

$$f \sim \left(R^{f,n}_S\right)^a \left(R^{f,n}_\rho\right)^b. \tag{2}$$

Thus

$$F^f_{S,n} \sim \frac{|\delta w_S|^f_n}{h_n} \left(|\delta w_S|^f_n h^3_n\right)^a \left(\frac{|\delta w_T|^f_n}{|\delta w_S|^f_n}\right)^b \tag{3a}$$

or

$$F^f_{S,n} = C\left(|\delta w_S|^f_n\right)^{1+a-b} \left(|\delta w_T|^f_n\right)^b h^{3a-1}_n \tag{3b}$$

To determine the exponents a and b, we take the logarithm of equation (3*b*) and re-arrange to display linear equations in a and b:

$$Z_n = aX_n + bY_n, \tag{4.1}$$

where

$$Z_n = \ln F^f_{s,n} - \ln C - \ln |\delta w_S|^f_n + \ln h_n,$$

$$X_n = \ln |\delta w_S|^f_n + 3 \ln h_n,$$

$$Y_n = -\ln |\delta w_S|^f_n + \ln |\delta w_T|^f_n.$$

A least-squares fit of the data to the linear regression equation gives a and b.

There were a total of 44 salt finger layers for which we had the complete set of data, δw_S, δw_T, h. We determined a, b using both subsets of the 44, and the complete set of 44, with the following results:

$N = 42$, using all but two sets with $h = 1\,\text{m}$:

$$a = 0.181, \quad b = 1.831;$$

$N = 31$, using only those with $h \leqslant 3\,\text{cm}$:

$$a = 0.188, \quad b = 2.126;$$

$N = 12$, using only those with $100\,\text{cm} > h \geqslant 3.5\,\text{cm}$:

$$a = 0.0198, \quad b = 1.718;$$

$N = 44$, using the complete set:

$$a = 0.107, \quad b = 1.865.$$

Since $h = 100\,\text{cm}$ represents fingers from the top to the bottom reservoir and could not be considered a staircase, we state that for the thermohaline staircase

$$a = 0.18 \text{ to } 0.19, \quad b = 1.8 \text{ to } 2.1.$$

Likewise, the salt flux across the nth convection zone may be expressed as

$$F^c_{S,n} = \kappa_S \frac{\delta w^c_{S,n}}{d_n} g(R^{c,n}, \tau, Pr), \tag{5}$$

where $\delta w^c_{S,n}$ is the salinity drop across the nth convection layer; d_n is the depth of the nth convection layer; g is a function of the dimensionless numbers $R^{c,n}$, the density Rayleigh number of the nth convection layer,

$$R^{c,n} = \frac{g}{\kappa_T \nu} \frac{\delta\rho_n}{\rho_0} d_n^3$$

and

$$\frac{\delta\rho_n}{\rho_0} = |\delta w_S|_n - |\delta w_T|_n.$$

Writing $g(R^{c,n})$ as a power law, $g \sim (R^{c,n})^a$ gives

$$F^c_{S,n} \sim |\delta w_S|^c_n \left(|\delta w_S|^c_n - |\delta w_T|^c_n\right)^a \left(d^c_n\right)^{3a-1}. \tag{6}$$

Of course, all the layers in the staircase are coupled and influence each other, as they are all part of a continuous fluid. Yet we may think in steps, with the flux out of the nth finger layer determining w_S and w_T at the top of the $(n+1)$th convection layer. Here, it is the difference $|\delta w_S| - |\delta w_T|$ across the convection layer, which, if positive, drives the convection; it, along with d_{n+1} and the material properties of the fluid, characterizes the convection in the $(n+1)$th layer. We might ask how much S and how much T are transported by this convection, especially as each may have a different boundary layer. The interior of this layer appears to be well-mixed (at least when observed as a horizontal average), so any difference in transport must be determined ultimately by the boundary layers. We attribute to the finger layers the role of convection boundary layers, and these finger layers are known to transport more S than T. However, within this model we may think of the well-mixedness of both T and S as signifying that they are equally transported by the convecting layer, in proportion to the ΔS and ΔT imposed.

It is noted that F_S increases with R_ρ as in the theory of Kunze 1987, where individual fingers do not fill the interface. Similarly, the data from the convection layer showed that

$$a = 0.21, \quad \text{i.e.} \quad N^c_S \sim R^{0.21},$$

for layer depths in the range $d = 5$ to 10 cm. For depth in the range $d = 10$ to 20 cm, $a = 0.16$.

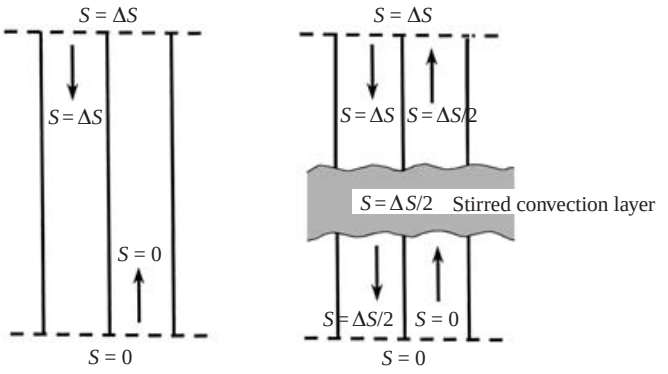

FIGURE 12. A schematic model of the drop in S-flux when coherent fingers are stirred by convection layers.

5. Discussion

Figure 9 shows that the Nusselt number increased by a factor of 3 from its value at $n = 8$ to its value at $n = 1$. The flux F_S also increased by a factor of 3, while ΔS overall dropped by 25%. One of the factors that could contribute to the increase of F_S with decrease of n is depicted in figure 12. Suppose that vertically coherent salt fingers flow between reservoirs at salinity ΔS at the top and zero at the bottom, with negligible lateral diffusion of salt. The salt flux $F_S^{(0)}$ would be proportional to $W\Delta S$, where W is an appropriately averaged vertical velocity.

On the other hand, if the vertical coherence were destroyed by stirring, say at mid-depth, and if the remaining fingers had the same W and finger width, then clearly the salt flux would be decreased. If the stirring produced perfect mixing of the sinking ΔS fluid and the rising $S = 0$ fluid, then $\Delta S/2$ would be carried in the up-finger from mid-depth to the top reservoir, thus returning half of the original export. If there were n such mixing layers, it is easy to show that the flux would drop to $1/n$ of $F_S^{(0)}$. This argument is for fixed ΔS. In figure 9 we show a curve $N_S \sim 1/n$ chosen to fit part of the data.

Now the convecting layers may or may not approximate perfect mixers, depending upon the Rayleigh numbers of these layers. At low enough Rayleigh numbers, convection with cellular structures would have vertical boundary-layer-like cell walls which approximate vertically coherent channels for the transport of S. At high enough Rayleigh numbers, large-scale flows set in (Krishnmurti & Howard 1981) which tend to eliminate lateral periodicities like cell walls. The Rayleigh numbers of these layers are of order 10^7 to 10^{10}, and are primarily determined by their depths d_i. Here there are two competing effects. First is the total number n of finger interfaces (per metre of tank depth, say). The larger n is, the smaller d_i is. Secondly, for fixed n, there is the ratio of finger height h_i to convecting layer depth d_i. The smaller h_i/d_i is, the larger the Rayleigh number of the ith convecting layer is. Thus it is conceivable that the flux law as shown in figure 9 would not vary exactly as $1/n$ but show a more complicated dependence on n as d_i varies with h_i as well as with n. More experimentation is required, especially with a tank whose sidewalls are not the restricting factor.

The overall flux measurements made in the stirred reservoirs (figure 9) are from data with four significant figures, whereas the internal measurements of refractive index η and optical rotation ϕ have only two significant figures. The variation of flux, which appears as a scatter of data at fixed n, seen in figure 9 is a real fluctuation associated

with merging finger zones and internal re-arrangement of the fluid following such a merger. On the other hand, the scatter in the data of Z_n, X_n, Y_n in equation (5) is from lack of precision. In summary, quantities such as ρ and S were measured to $\pm 0.01\%$ but the final determination of the exponents a, b showed variations on the order of 10% depending on the selection of interface heights to be included.

We did attempt to use here the method employed by Schmitt 1979 and McDougall & Taylor 1984, and others who determined fluxes across a single finger interface by measuring the change in salinity with time of the convecting zones. Our measurement in the reservoirs uses this same method. However, when applied to one of the many internal convection zones it worked less well. There was always a vertical jump in w_S across finger interfaces, indicating vertical flux of Su, but often there was apparently no flux divergence to cause w_S to change with time. When there was change, it did not vary smoothly in time, but was associated with mergers and post-merger re-arrangements.

The convective flux laws show a strong dependence upon layer depth, that is, on aspect ratio A as well as on Rayleigh number. When the convecting layers were relatively deep and $Ra \sim 10^{10}$, the power law $N_T \sim Ra^a$ gave $a = 0.21$ in agreement with that found in Rayleigh–Bénard convection at large A (Krishnamurti 1995). However, as the finger zones grew and convection zones waned ($Ra \sim 10^7$ to 10^8), the power a decreased to as low as $a = 0.16$. Our next experiment will be to determine flux laws in a tank 0.3 m deep but with horizontal dimensions 15 by 150 cm.

With quantities such as T and S governed by second-order differential equations, it would seem that specifying values at two boundaries would be sufficient, while here we have specified the initial internal profile as well. There are two ways of justification. The first is the practical matter of time limitation. Specifying Su, Sa on the boundaries and waiting for diffusion to produce the interior profiles could require 100 years in the 2 m tank, 3 years in the 0.3 m tank. In the 0.3 m tank, we did trials with only the Sa profile specified in the interior and Su supplied from the top boundary. After some weeks, the flow and fluxes looked identical to those when both profiles were initially specified.

The second consideration is that in natural occurrences, such as in the sub-tropical oceans, other processes not modelled here may be continuously producing these mean vertical profiles. Thus for example, the horizontal North–South temperature gradient and associated water mass formation at the surface may become imprinted in the vertical in the wind-driven gyre circulation.

6. Conclusions

For overall Rayleigh numbers R_S and R_T in the range -10^{12} to -10^{15} and density ratio R_ρ in the range 1.1 to 1.3, the main results are as follows:

1. Flow visualization showed many distinctive flow regimes, which could be roughly categorized as follows:

(i) straight fingers, (ii) lumpy fingers, (iii) wavy fingers, (iv) staircases of alternating finger and convection layers; within the staircase, the finger layer could show the above forms as well. PIV and PTV images of the flow within a vertical (x, z)-plane are consistent with interpretations of corresponding shadowgraphs which average in the horizontal (y) direction.

2. Overall flux measurements F_S and F_T in the staircase regime are definitely not depth independent. For the same ΔS, ΔT imposed between top and bottom reservoirs, the 0.3 m tank generally had the largest flux, then the 1 m tank; the 2 m tank had the smallest flux even though its overall Rayleigh numbers are clearly largest and the

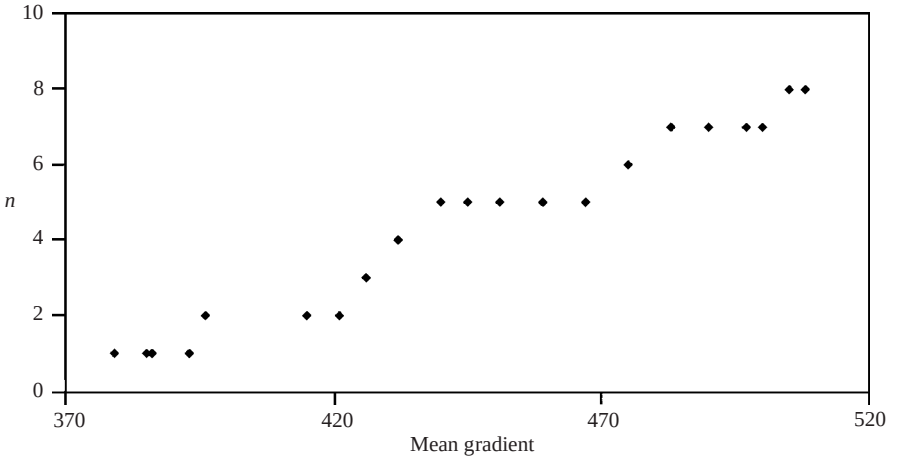

FIGURE 13. The number n of interfaces versus the mean sugar gradient (arbitrary units) across the total depth of the tank. The numbers on the abscissa when multiplied by 5.38×10^{-3} give the mean sugar gradient in g l^{-1} per cm of depth.

0.3 m tank's clearly the smallest. When there are many layers, the overall Nusselt number N_S is not expressible as $N_S \sim |R_S|^a$ with any positive power a.

The main result regarding the overall Nusselt number is that it varies inversely with the number n of finger interfaces across the depth through which ΔS is imposed. As n decreases, N increases. The number n varies in a monotonic but step-like manner with the imposed gradient (figure 13) (and thus with overall Rayleigh number). Large enough gradients inhibit staircase formation. Vertically coherent fingers have the largest Nusselt numbers, while increased numbers of convecting layers lead to decreased Nusselt numbers.

3. Internal flux measurements for salt across finger interfaces are expressed as

$$F^f_{S,i} \sim \frac{\Delta S_i}{h_i} |R_{S,i}|^a |R_{\rho,i}|^b$$

for the ith layer. A least-squares fit to a linear regression equation gives

$$a = 0.18 \text{ to } 0.19, \quad b = 1.8 \text{ to } 2.1.$$

Since a is not equal to $\frac{1}{3}$, there is a dependence of $F^f_{S,i}$ on h_i. The convective layers have Rayleigh number $R > 0$ and

$$N_S \sim R^{0.21}$$

for large enough aspect ratio.

I wish to acknowledge many helpful discussions with George Veronis, L. N. Howard, Melvin Stern, David Loper, David Furbish, and Robin Kung. I am especially grateful to Professor Ron Adrian for providing us with the data analysis program PIV Sleuth, and to T. N. Krishnamurti and his staff for help with computing problems. This research was supported in part by the National Science Foundation under grant number OCE-9809805. This is contribution number 431 of the Geophysical Fluid Dynamics Institute at Florida State University.

REFERENCES

Castaing, B., Gunarantne, G., Heslot, F., Kadanoff, L., Libchaber, A., Thomae, S., Wu, X.-Z., Zaleski, S. & Zanetti, G. 1989 Scaling of hard thermal turbulence in Rayleigh–Benard convection. *J. Fluid Mech.* **204**, 1–30.

Christiansen, K. T., Soloff, S. M. & Adrian, R. J. 2001 PIV Sleuth: Integrated Particle Image Velocimetry (PIV) Interrogation/Validation Software. *Tech. Rep.* 943. Department of Theoretical and Applied Mechanics, University of Illinois at Urbana-Champaign (2000).

Dougherty, R. C. 2001 Density of salt solutions: effect of ions on the apparent density of water. *J. Phys Chem.* **105**, 4514–4519.

Goldstein, R. J., Chaing, J. D. & See, D. L. 1990 High-Rayleigh-number convection in horizontal enclosure. *J. Fluid Mech.* **213**, 111–126.

Krishnamurti, R. 1995 Low-frequency oscillations in turbulent Rayleigh-Benard convection: laboratory experiments. *Fluid Dyn. Res.* **16**, 87–108.

Krishnamurti, R. & Howard, L. N. 1981 Large-scale flow generation in turbulent convection. *Proc. Natl Acad. Sci.* **78,** 1981–1985.

Krishnamurti, R. & Zhu, Y. 1989 Double diffusive convection with imposed vertical mass flux. *J. Mar. Res.* **48**, 1–21.

Kunze, E. 1987 Limits on growing, finite-length salt-fingers: a Richardson Number constraint. *J. Mar. Res.* **45**, 533–556.

Linden, P. F. 1973 On the structure of salt fingers. *Deep-Sea Res.* **20,** 325–340.

Linden, P. F. 1978 The formation of banded salt finger structure. *J. Geophys. Res.* **83**, 2902–2912.

McDougall, T. J. & Taylor, J. R. 1984 Flux measurements across a finger interface at low values of the stability ratio. *J. Mar. Res.* **42**, 1–14.

Molcard, R. & Williams, A. J. 1975 Deep stepped structure in the Tyrrhenian Sea. *Mémoire Société Royale des Sciences de Liège,* 6^{e} *périe* **VII**, 191–210.

Ruddick, B. R. & Shirtcliffe, T. G. L. 1979 Data for double diffusers: physical properties of aqueous salt-sugar solutions. *Deep-Sea Res.* **26A**, 775–7873.

Schmitt, R. W. 1979 Flux measurements at an interface. *J. Mar. Res.* **37**, 419–436.

Shirtcliffe, T. G. L. & J. S. Turner, J. S. 1970 Observations of the cell structure of salt fingers. *J. Fluid Mech.* **41**, 707–719.

Stern, M. E. 1969 Collective instability of salt fingers. *J. Fluid Mech.* **35**, 209–218.

Stern, M. E. & Turner, J. S. 1969 Salt fingers and convecting layers. *Deep-Sea Res.* **16**, 497–511.

Turner, J. S. 1967 Salt fingers across a density interface. *Deep-Sea Res.* **14**, 599–611.